Eur. Phys. J. C 25, 539–551 (2002)
Digital Object Identifier (DOI) 10.1007/s10052-002-1027-6

THE EUROPEAN PHYSICAL JOURNAL C

Associated production of sfermions and gauginos at high-energy e^+e^- colliders: The case of selectrons and electronic sneutrinos

Aseshkrishna Datta, A. Djouadi, M. Mühlleitner

Laboratoire de Physique Mathématique et Théorique, UMR5825-CNRS, Université de Montpellier II, 34095 Montpellier Cedex 5, France

Received: 27 June 2002 /
Published online: 20 September 2002 –

Abstract. We analyze the associated production at future high-energy e^+e^- colliders, of first generation sleptons with neutralinos and charginos in the modes e^+e^- and $e\gamma$, in the framework of the minimal supersymmetric extension of the standard model. We show that the production rates, in particular for associated production of right-handed selectrons and the lightest neutralino which in general is the first accessible kinematically, can be much larger than the corresponding ones for second and third generation scalar leptons and for scalar quarks. With the high luminosities expected at these colliders, the detection of first generation sleptons with masses significantly above the kinematical two-body threshold, $s^{1/2} = 2m_{\tilde{\ell}}$, is thus possible in favorable regions of the parameter space.

1 Introduction

In a preceding paper [1], the associated production of scalar fermions with neutralinos and charginos at future high-energy e^+e^- colliders has been analyzed in the context of the minimal supersymmetric standard model (MSSM). For scalar leptons, only the cases of left- and right-handed smuons, staus and their partner sneutrinos have been considered. The associated production of scalar quarks, including the lightest third generation states, $\tilde{t}_1$ and $\tilde{b}_1$, with neutralinos, charginos as well as with gluinos, have also been studied. It has been shown that some of these three-body processes can have production cross sections sizeable enough to allow for the possibility of discovering sfermions with masses slightly above the kinematical threshold for pair production at $\mathcal{O}(1\,\text{TeV})$ e^+e^- colliders, i.e. $s^{1/2} = 2m_{\tilde{f}}$, in favorable regions of the supersymmetric (SUSY) parameter space.

The case comprising of associated production of first generation sleptons, left- and right-handed selectrons $\tilde{e}_{\rm L,R}$ and electronic sneutrinos $\tilde{\nu}_e$, with charginos and neutralinos is more complicated compared to the case of second and third generation sleptons. This is mostly due to the fact that, because of the possibility of t-channel exchange of charginos and neutralinos in the two-body production processes, $e^+e^- \to \tilde{e}_{\rm L/R}\tilde{e}_{\rm L/R}$ and $e^+e^- \to \tilde{\nu}_e\tilde{\nu}_e$, respectively, there are many more contributing Feynman diagrams for the three-body final states, $e^+e^- \to \ell_e\tilde{\ell}_e\chi$. In addition, there are extra contributions with diagrams involving the exchange of γ, Z, W gauge bosons in the t-channel. Particularly important are those with t-channel γ exchange, which for almost real photons, lead to poles that need to be handled carefully.

In the present paper, we extend the analysis of [1] to include the case of associated production of first generation scalar leptons with the lighter charginos and neutralinos. We first investigate the associated production of selectrons and sneutrinos with the lighter neutralinos, $\chi^0_{1,2}$, or chargino, $\chi^\pm_1$, states in electron–photon collisions [2,3]

$$\gamma e^\pm_{\rm L,R} \to \tilde{e}^\pm_{\rm L,R}\chi^0_{1,2}, \quad \gamma e^\pm_{\rm L,R} \to \tilde{\nu}_e\chi^\pm_1 \tag{1}$$

for real photons coming from the initial electron/positron beams in the original [4] and improved [5] Weizsäcker–Williams approximations, as well as in the case of an $e\gamma$ collider with the photon generated by Compton back scattering of laser light [6]. We then analyze the three-body processes for selectron and sneutrino productions

$$\begin{aligned} &e^+e^- \to e^\pm\tilde{e}^\mp_{\rm L,R}\chi^0_{1,2}, \quad e^+e^- \to \nu\tilde{e}^\pm_{\rm L,R}\chi^\mp_1, \\ &e^+e^- \to \nu_e\tilde{\nu}_e\chi^0_{1,2}, \quad e^+e^- \to e^\pm\tilde{\nu}\chi^\mp_1 \end{aligned} \tag{2}$$

in the e^+e^- mode of a future linear collider with c.m. energies $s^{1/2} = 500\,\text{GeV}$ and $1\,\text{TeV}$.

2 Production in the $e\gamma$ mode

The associated production of selectrons with neutralinos and sneutrinos with charginos in $e^-\gamma$ collisions [the cross sections are the same in $e^+\gamma$ processes because of CP-invariance] occur through the s-channel exchange of electrons and the t-channel exchange of selectrons or charginos; see Fig. 1.

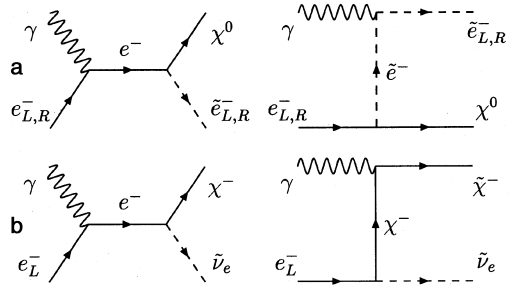

Fig. 1a,b. Feynman diagrams contributing to the associated production of selectrons with neutralinos **a** and sneutrinos with charginos **b** in $e^-\gamma$ collisions

The cross sections of the subprocesses for longitudinally polarized electrons and unpolarized photons are as follows:

$$\begin{aligned}
&\hat{\sigma}(e^-_{\mathrm{L,R}}\gamma \to \tilde{e}^-_{\mathrm{L,R}}\chi^0_i)\\
&= \frac{\pi\alpha^2}{2\hat{s}^3}|G^i_{\mathrm{L,R}}|^2\left[(\hat{s}-7m^2_{\chi^0_i}+7m^2_{\tilde{e}_{\mathrm{L,R}}})\sqrt{\lambda}\right.\\
&- 4(m^2_{\tilde{e}_{\mathrm{L,R}}}-m^2_{\chi^0_i})(\hat{s}+m^2_{\tilde{e}_{\mathrm{L,R}}}-m^2_{\chi^0_i})\\
&\times \left.\ln\left(\frac{\hat{s}-m^2_{\chi^0_i}+m^2_{\tilde{e}_{\mathrm{L,R}}}+\sqrt{\lambda}}{\hat{s}-m^2_{\chi^0_i}+m^2_{\tilde{e}_{\mathrm{L,R}}}-\sqrt{\lambda}}\right)\right], \qquad (3)\\
&\hat{\sigma}(e^-_{\mathrm{L}}\gamma \to \tilde{\nu}_{\mathrm{L}}\chi^-_i)\\
&= \frac{\pi\alpha^2}{2\hat{s}^3}|G^i|^2\left[(-3\hat{s}-7m^2_{\chi^-_i}+7m^2_{\tilde{\nu}_{\mathrm{L}}})\sqrt{\lambda}\right.\\
&+ 2(\hat{s}^2+2m^2_{\chi^-_i}\hat{s}-2m^2_{\tilde{\nu}_{\mathrm{L}}}\hat{s}+2(m^2_{\chi^-_i}-m^2_{\tilde{\nu}_{\mathrm{L}}})^2)\\
&\times \left.\ln\left(\frac{\hat{s}+m^2_{\chi^-_i}-m^2_{\tilde{\nu}_{\mathrm{L}}}+\sqrt{\lambda}}{\hat{s}+m^2_{\chi^-_i}-m^2_{\tilde{\nu}_{\mathrm{L}}}-\sqrt{\lambda}}\right)\right], \qquad (4)
\end{aligned}$$

where $\hat{s}$ is the $e\gamma$ c.m. energy and λ, the two-body phase space function, given by

$$\begin{aligned}
\lambda &\equiv \lambda(\hat{s}, m^2_{\tilde{\ell}}, m^2_{\chi_i})\\
&= \hat{s}^2 + m^4_{\tilde{\ell}} + m^4_{\chi_i} - 2\hat{s}m^2_{\tilde{\ell}} - 2\hat{s}m^2_{\chi_i} - 2m^2_{\tilde{\ell}}m^2_{\chi_i}. \qquad (5)
\end{aligned}$$

$G^i_{\mathrm{L,R}}$ (G^i) denote the selectron–neutralino–electron (sneutrino–chargino–electron) couplings; in terms of $s^2_{\mathrm{W}} = 1 - c^2_{\mathrm{W}} \equiv \sin^2\theta_{\mathrm{W}}$ and for $i = 1, 2$, they are given by

$$\begin{aligned}
G^i_{\mathrm{L}} &= \frac{1}{\sqrt{2}}\left(\frac{N_{i1}}{c_{\mathrm{W}}} + \frac{N_{i2}}{s_{\mathrm{W}}}\right), \quad G^i_{\mathrm{R}} = -\frac{\sqrt{2}}{c_{\mathrm{W}}}N_{i1},\\
G^i &= -\frac{1}{s_{\mathrm{W}}}V_{i1}, \qquad (6)
\end{aligned}$$

where N is the matrix which diagonalizes the 4×4 neutralino matrix while V is one of the unitary matrices which diagonalize the 2×2 chargino mass matrix [7,8].

The cross sections of the full processes $e^+e^- \to e^+\tilde{e}^-_{\mathrm{L,R}}\tilde{\chi}^0_i$ and $e^+e^- \to e^+\tilde{\nu}_{\mathrm{L}}\tilde{\chi}^-_i$ are obtained by folding the cross sections of the subprocesses (3) and (4), respectively, with the photon luminosity $P_{\gamma/e}(y)$, in which s denotes the total e^+e^- c.m. energy and y the fraction of the electron energy carried by the photon:

$$\sigma(e^+e^- \to e^+\tilde{\ell}\chi_i) = \int_{y^-}^{y^+} \mathrm{d}y\; P_{\gamma/e}(y)\hat{\sigma}(\hat{s} = ys). \qquad (7)$$

In our analysis, we will discuss three possibilities for the photon luminosity.

(a) The Weizsäcker–Williams (WW) spectrum [4]

$$P_{\gamma/e}(y) = \frac{\alpha}{2\pi}\frac{1+(1-y)^2}{y}\ln\frac{s}{m^2_e}, \qquad (8)$$

with the electron mass $m_e = 510.99906\,\mathrm{keV}$ and the integration boundaries

$$y^- = (m^2_{\tilde{\ell}} + m^2_{\chi_i})/s, \quad y^+ = 1. \qquad (9)$$

In general, this approximation overestimates the production cross sections.

(b) The improved Weizsäcker–Williams approximation [5] is more reliable than the original WW approximation for small enough θ_c values, where θ_c denotes the angle between the direction of the positron before and after radiating off a photon [outgoing positrons above the angular cut θ_c compared to the initial direction of the beam are eliminated]. Denoting the electron (beam) energy by $E = s^{1/2}/2$, the spectrum is given by

$$\begin{aligned}
P_{\gamma/e}(y) = \frac{\alpha}{2\pi}\Bigg[&2(1-y)\left(\frac{m^2_e y}{E^2(1-y)^2\theta^2_c + m^2_e y^2} - \frac{1}{y}\right)\\
&+ \frac{1+(1-y)^2}{y}\ln\frac{E^2(1-y)^2\theta^2_c + m^2_e y^2}{m^2_e y^2}\\
&+ \mathcal{O}(\theta_c, m^2_e/E^2)\Bigg] \qquad (10)
\end{aligned}$$

(c) The Compton back-scattering spectrum [6]

$$P_{\gamma/e}(y) = \frac{1}{\sigma_c}\frac{\mathrm{d}\sigma_c(y)}{\mathrm{d}y}, \qquad (11)$$

with the differential Compton cross section

$$\frac{\mathrm{d}\sigma_c}{\mathrm{d}y} = \frac{\pi\alpha^2}{xm^2_e}[f_0 + P_eP_\gamma f_1 + P_eP_{\gamma'}f_2 + P_\gamma P_{\gamma'}f_3]; \qquad (12)$$

$P_e, P_\gamma, P_{\gamma'}$ denote the helicities of the initial electron, the laser photon γ and the scattered photon γ', respectively, with $-1 \le P_e, P_\gamma, P_{\gamma'} \le 1$. The parameter x is given by $x = 4E\omega_0/m^2_e$ with $E = s^{1/2}/2$ and the laser energy is $\omega_0 = 1.26\,\mathrm{eV}$. In terms of $r = y/(x(1-y))$, the functions f_i ($i = 0, ..., 3$) read

$$\begin{aligned}
f_0 &= \frac{1}{1-y} + 1 - y - 4r(1-r),\\
f_1 &= xr(1-2r)(2-y),\\
f_2 &= xr(1+(1-y)(1-2r)^2),\\
f_3 &= (1-2r)\left(\frac{1}{1-y} + 1 - y\right). \qquad (13)
\end{aligned}$$

The integrated Compton cross section σ_c can be cast into the form

$$\begin{aligned}\sigma_c &= \sigma_c^{\rm np} + P_e P_\gamma \sigma_c^{\rm p},\\ \sigma_c^{\rm np} &= \frac{\pi\alpha^2}{x m_e^2}\left[\frac{1}{2}+\frac{8}{x}-\frac{1}{2(1+x)^2}\right.\\ &\quad\left.+\left(1-\frac{4}{x}-\frac{8}{x^2}\right)\ln(x+1)\right],\\ \sigma_c^{\rm p} &= \frac{\pi\alpha^2}{x m_e^2}\left[-\frac{5}{2}+\frac{1}{x+1}-\frac{1}{2(x+1)^2}\right.\\ &\quad\left.+\left(1+\frac{2}{x}\right)\ln(x+1)\right], \end{aligned} \tag{14}$$

with the integration boundaries in this case given by

$$y^- = (m_{\tilde\ell}^2 + m_{\chi_i}^2)/s, \quad y^+ = x/(x+1). \tag{15}$$

In $e\gamma$ colliders, with the photon generated by Compton back-scattering of laser light, c.m. energies of the order of 80 to 90% of the e^+e^- collider energy, integrated luminosities $\int\mathcal{L}\sim 200\,{\rm fb}^{-1}$, and a high degree of longitudinal photon polarization can be reached [9].

The production cross sections of selectrons and sneutrinos in association with, respectively, the two lightest neutralinos $\chi^0_{1,2}$ and the lighter chargino $\chi^\pm_1$ are shown as functions of the slepton masses in Figs. 2 for the three options of the photon luminosity discussed above: (a) for the WW approximation, (b) for the improved WW approximation with an angular cut $\theta_c = 1^\circ$ and (c) for the Compton collider. The e^+e^- c.m. energies are set to 500 GeV (left panel) and 1 TeV (right panel) as expected for the next generation colliders [10]. The initial e^- is assumed to be polarized longitudinally: left-handed polarization for the production of $\tilde e_{\rm L}$ and $\tilde\nu_e$ and right-handed polarization for the production of $\tilde e_{\rm R}$. The degrees of polarization are assumed to be equal to one, close to the value expected (80 to 90%) at machines such as TESLA [10]. Note that only processes involving the $e^-\gamma$ initial state are taken into account in the cross sections of Fig. 2a,b; inclusion of the charge conjugate processes with $e^+\gamma$, would lead to cross sections which are larger by a factor of 2 [if the degree of polarization of the e^+ beam is the same as for the e^- beam].

For the SUSY parameters, we have chosen $\tan\beta = 30$, the higgsino mass parameter $\mu = 500$ GeV and the gaugino masses at the weak scale $M_1 = 50$ and $M_2 = 100$ GeV, which implies approximate unification at the GUT scale. This leads to gaugino-like lighter charginos and neutralinos with masses $m_{\chi^0_1}\simeq M_1$ and $m_{\chi^0_2}\simeq m_{\chi^\pm_1}\simeq M_2$, i.e. around the experimental limits from LEP2 negative searches [11]. This choice is motivated by the fact that in this limit, the selectron–electron–$\chi^0_{1,2}$ and sneutrino–electron–χ^-_1 couplings (6) are maximal. For mixed gaugino and higgsino states, i.e. for $|\mu|\sim M_2$, these couplings are suppressed and vanish in the higgsino-like limit $|\mu|\ll M_2$ [the higgsino couplings to electrons and sleptons are proportional to the electron mass]. We will not discuss the case of associated production of the heavier chargino and neutralino states with sleptons which are disfavored by phase space. In particular, for the case of interest, i.e. for $M_2 \ll |\mu|$, the heavier chargino and neutralino states are higgsino-like with large masses $m_{\chi^0_3}\sim m_{\chi^0_4}\sim m_{\chi^\pm_2}\simeq|\mu|$ and in addition, they have tiny couplings to electron–slepton pairs. For more details, see the discussion given in [1]. Note also that the cross section for the process $e^-\gamma\to\tilde e^-_{\rm R}\chi^0_2$ vanishes in the limit of gaugino-like next-to-lightest neutralinos since the right-handed selectron does not couple to the winos.

For the e^+e^- option with Weizsäcker–Williams photons, Fig. 2a,b, the cross sections in the original approximation are about a factor of two larger than in the improved approximation with the angle θ_c between the initial and the final positron set to 1°. The cross section in the improved WW approximation vanishes at $\theta_c = 0$ [since the photon luminosity in (10) goes to zero] and increases with increasing θ_c [some illustrative examples will be given later on]. In the chosen scenario, for slepton masses only slightly above the threshold for pair production in e^+e^- collisions, $s^{1/2}\sim 2m_{\tilde\ell}$, and fairly far from the kinematical limit in associated production, $s^{1/2}\sim m_{\tilde\ell}+m_\chi$, the gaugino mass effects do not play a significant role and the cross sections for selectron production are such that

$$\begin{aligned}&\sigma(e_{\rm L}\gamma\to\tilde e_{\rm L}\chi^0_2)/\sigma(e_{\rm L}\gamma\to\tilde e_{\rm L}\chi^0_1)\sim 3,\\ &\sigma(e_{\rm R}\gamma\to\tilde e_{\rm R}\chi^0_1)/\sigma(e_{\rm L}\gamma\to\tilde e_{\rm L}\chi^0_1)\sim 4.\end{aligned} \tag{16}$$

These are simply the ratios of the squares of the selectron–electron–gaugino couplings in the gaugino limit, $(G^2_{\rm L})^2/(G^1_{\rm L})^2\sim 3$ (for $s^2_{\rm W}\simeq 1/4$) and $(G^1_{\rm R})^2/(G^1_{\rm L})^2 = 4$. The behaviors of the cross sections are almost identical except for the more rapid fall-off for higher masses for $\sigma(e_{\rm L}\gamma\to\tilde e_{\rm L}\chi^0_2)$, because of a fast reducing phase space [$m_{\chi^0_2}\simeq 2m_{\chi^0_1}$].

At a 500 GeV e^+e^- collider, the cross sections are of the order of 0.6 (2.6) fb for $e_{\rm L(R)}\gamma\to\tilde e_{\rm L(R)}\chi^0_1$ for selectron masses of $m_{\tilde\ell_{\rm L,R}}\sim 275$ GeV in the WW approximation. This means that 300 (1300) events can be collected for a yearly integrated luminosity of $\int\mathcal{L} = 500\,{\rm fb}^{-1}$ as expected for a machine like TESLA. Even for masses of about $m_{\tilde\ell}\sim 400$ GeV, i.e. far above the mass reach for slepton pair production, the cross section for $\tilde e_{\rm R}\chi^0_1$ production is of the order of 0.1 fb which means that approximately 100 events can be collected in two years of running, a sample which might be sufficient to discover these particles in the clean environment of e^+e^- colliders. The cross sections will of course be smaller for increasing values of the gaugino masses as will be illustrated later.

The cross section for sneutrino–chargino production is an order of magnitude larger than the largest cross section for selectrons, $\sigma(e_{\rm R}\gamma\to\tilde e_{\rm R}\chi^0_1)$; for low slepton masses, it exceeds the level of 10 fb (for $m_{\tilde\nu} = 300$ GeV) at $s^{1/2} = 500$ GeV. This is mainly due to the fact that the magnitude of charged currents is larger than the one for neutral currents, but also because in the t-channel diagrams, it is a lighter chargino which is exchanged in this case [compared to the slepton in the previous case]. The

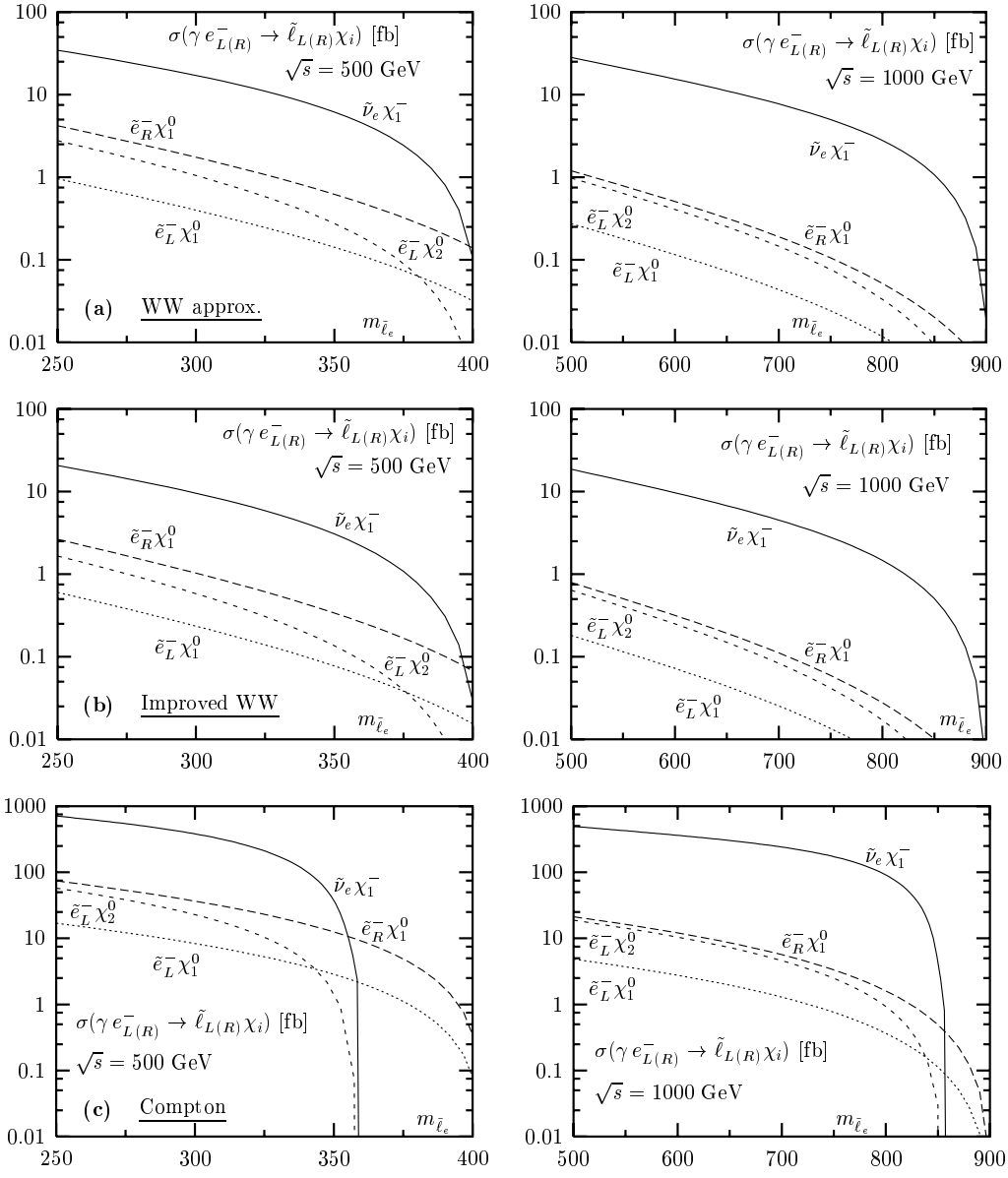

Fig. 2a–c. Total cross sections for the associated production of first generation sleptons with charginos and neutralinos in $e^-\gamma$ collisions as functions of the slepton masses for c.m. energies of 500 GeV (left panel) and 1 TeV (right panel) in the WW approximation, improved WW approximation and for a Compton collider

latter feature also explains the slightly different behaviors of the cross sections for higher slepton masses.

The cross sections are also shown for an e^+e^- c.m. energy of 1 TeV and slepton masses above 500 GeV. While in the case of selectrons they are smaller by a factor 3 to 4 [the s-channel electron exchange contribution scales like $1/s$ and is therefore smaller] for a fixed $m_{\tilde{\ell}}/s^{1/2}$ value, the cross sections stay approximately the same for sneutrino–chargino production because of the dominance of the chargino t-channel exchange.

Finally, the cross sections in the $e\gamma$ mode of the e^+e^- collider, with the photon generated by Compton backscattering, are shown in Fig. 2c. The laser energy is taken to be 1.26 eV, leading to a parameter $x = 4.83$ and $x = 9.65$ for the c.m. energies of the initial e^+e^- machine of 500 GeV and 1 TeV, respectively. For relatively low slepton masses, the cross sections are more than one order of magnitude larger than in the Weizsäcker–Williams approximation, with the ratios between cross sections with different states being approximately the same. This means that if the luminosity of the $e\gamma$ collider is of the same order as the luminosity of the e^+e^- colliders, a very large number of events can be collected. However, there is a very strong fall-off of some of the cross sections for large slepton masses, in particular in the case of selectron and sneutrino production in association with χ_2^0 and $\chi_1^\pm$, respectively. Because the energy of the $e\gamma$ collider peaks at approximately 90% of the e^+e^- c.m. energy, the phase

space suppression becomes very strong for slepton masses close to $m_\ell \sim 350\,\text{GeV}$ at $s^{1/2}_{e^+e^-} = 500\,\text{GeV}$, since in this case, $m_{\chi^0_2} \sim m_{\chi^\pm_1} \sim M_2 = 100\,\text{GeV}$, leading to $m_\ell + m_{\chi_i} \sim 450\,\text{GeV}$.

Thus the cross sections for associated production of sleptons of the first generation along with the lighter charginos or neutralinos are significant, even in the e^+e^- option with Weizsäcker–Williams photons. Selectrons or sneutrinos with masses beyond the values which can be reached in pair production in e^+e^- collisions [approximately the beam energy] can be probed with high luminosities if the charginos and neutralinos are lighter. However, the accompanying electron/positron are in general not experimentally detected in this case. To take into account this possibility as well, the full three-body production process, $e^+e^- \to \ell\tilde{\ell}\chi_i$, to which we turn now, has to be considered.

3 Production in e^+e^- collisions

There is a large number of Feynman diagrams contributing to the associated production in e^+e^- collisions of first generation selectrons $\tilde{e}_{\text{L,R}}$ or sneutrinos $\tilde{\nu}_e$ with the lighter chargino $\chi^\pm_1$ or neutralinos $\chi^0_{1,2}$. Neglecting the exchange of the heavier chargino or neutralinos [which, as discussed previously, do not couple to the sleptons and leptons in the gaugino limit] one has: 28 Feynman diagrams for $e^+e^- \to e^+\tilde{e}^-_{\text{L,R}}\chi^0_i$, 17 diagrams for $e^+e^- \to \bar{\nu}_e\tilde{\nu}_e\chi^0_i$, 13 diagrams for $e^+e^- \to \nu_e\tilde{e}^-_{\text{L}}\chi^+_1$, 6 diagrams for $e^+e^- \to \nu_e\tilde{e}^-_R\chi^+_1$ and 12 diagrams for $e^+e^- \to e^+\tilde{\nu}_e\chi^-_1$. The set of generic diagrams contributing to the associated production of left- or right-handed selectrons with the neutralinos $\chi^0_{1,2}$ are shown in Fig. 3a–c. A similar set of diagrams appears in the other processes. These diagrams can be divided into three separately gauge invariant categories.

(a) Universal diagrams which occur also in the case of the associated production of second and third generation sleptons with electroweak gauginos [and as such, this set is therefore gauge invariant by itself]. The amplitudes are discussed in [1].

(b) Non-universal diagrams, i.e. those which are special to the case of first generation sleptons, and which do not involve the exchange of photons in the t-channel. They all involve neutralino or Z boson exchange in the t-channel [which does not occur for associated smuon production due to flavor conservation].

(c) Non-universal diagrams where a photon is exchanged in the t-channel. Here, the electron or positron radiates a photon and part of the reaction will be exactly the same as the one discussed previously for $e\gamma$ collisions, but with the photon being virtual.

Similar diagrams occur for the other associated production processes. Note that in the processes where charginos and sneutrinos are produced in association, $e^+e^- \to e^\pm\tilde{\nu}_e\chi^\mp_1$, there are also Feynman diagrams involving the t-channel exchange of photons, Fig. 3d, and corresponding to those discussed in the case of $e\gamma$ collisions but with the photon being virtual. Such diagrams with t-channel photons do not occur in the associated production of charginos with selectrons or neutralinos with sneutrinos.

The amplitudes for diagrams 3b, 3c and 3d are given in Appendix A, while the ones for diagrams 3a are already given in [1] from which we borrow the notation. The full analytical expression for the differential cross section is rather lengthy and not very telling. In Appendix B, we will however write down the expressions for the squared amplitude of the sum of the two contributions which involve the t-channel photon exchange only. This, as we will show later, is the most important one numerically. In the following, we will simply discuss our numerical results from the complete calculation. We note that in all cases, we have thoroughly cross checked our numerical results against the corresponding ones from the package CompHEP [12].

The total cross sections for the associated productions of first generation sleptons with the two lightest neutralinos χ^0_1 (a) and χ^0_2 (b) as well as with the lightest chargino $\chi^\pm_1$ (c) are shown in Fig. 4 as functions of the slepton mass and for two center of mass energies $s^{1/2} = 500\,\text{GeV}$ (left panel) and 1 TeV (right panel). As in the previous section, we have assumed a common soft-SUSY breaking mass for the scalars and fixed the SU(2) gaugino and higgsino mass terms to be $M_2 = 2M_1 = 100\,\text{GeV}$ and $\mu = 500\,\text{GeV}$ with $\tan\beta = 30$. The cross sections are displayed for unpolarized initial beams and the charged conjugate final states [which lead to a factor of 2 increase of the cross sections] have been included. In the case of $e^\pm\tilde{e}^\mp_{\text{L,R}}\chi^0_{1,2}$ and $e^\pm\tilde{\nu}_e\chi^\mp_1$ production, which involve the t-channel photon poles, we have applied a cut on the minimum angle between the direction of the final electron (positron) with respect to the incident electron (positron), $\theta_{\min} = 1^\circ$. This cut is used to avoid the numerical instabilities near the t-channel photon pole[1].

As can be seen, at $s^{1/2} = 500\,\text{GeV}$, the production cross sections can be rather large, exceeding the level of 0.1 fb for slepton masses close to $m_{\tilde{\ell}} \sim 350\,\text{GeV}$, except in the case of $\tilde{e}_\text{R}$ production with χ^0_2 and χ^+_1 [because $\tilde{e}_\text{R}$ has very small couplings to these dominantly SU(2) gauginos] and $\tilde{\nu}_e$ production with the LSP [because the bino–$\tilde{\nu}_e$–ν_e coupling is suppressed and there is no t-channel photon to enhance the rate]. The largest rates are obtained for the processes $e^+e^- \to e^\pm\tilde{e}^\mp_\text{R}\chi^0_1$ and $e^+e^- \to e^\pm\tilde{\nu}^{(*)}_e\chi^\mp_1$. This is due to the larger $\tilde{e}_\text{R}$ couplings to electrons and binos in the former case and because of the stronger charged current interactions for the latter, both of which are fortified with contributions from the t-channel photon exchange. For $m_{\tilde{\ell}} \sim 350\,\text{GeV}$ and $m_{\chi^+_1} \sim 2m_{\chi^0_1} \sim 100\,\text{GeV}$, the cross sections are at the level of 0.5 fb and 2 fb, respectively, allowing one to collect a few hundreds of events in each process with the expected luminosity of $\int\mathcal{L} \sim 500\,\text{fb}^{-1}$. [In fact, even for $m_{\tilde{\ell}} \sim 400\,\text{GeV}$, one can still produce a few

[1] In principle, one can regulate this pole by including the finite mass of the electron also in the phase space (as we have already done). However, since m_e is much smaller compared to $s^{1/2}$, a very delicate and lengthy Monte-Carlo phase space integration would be required

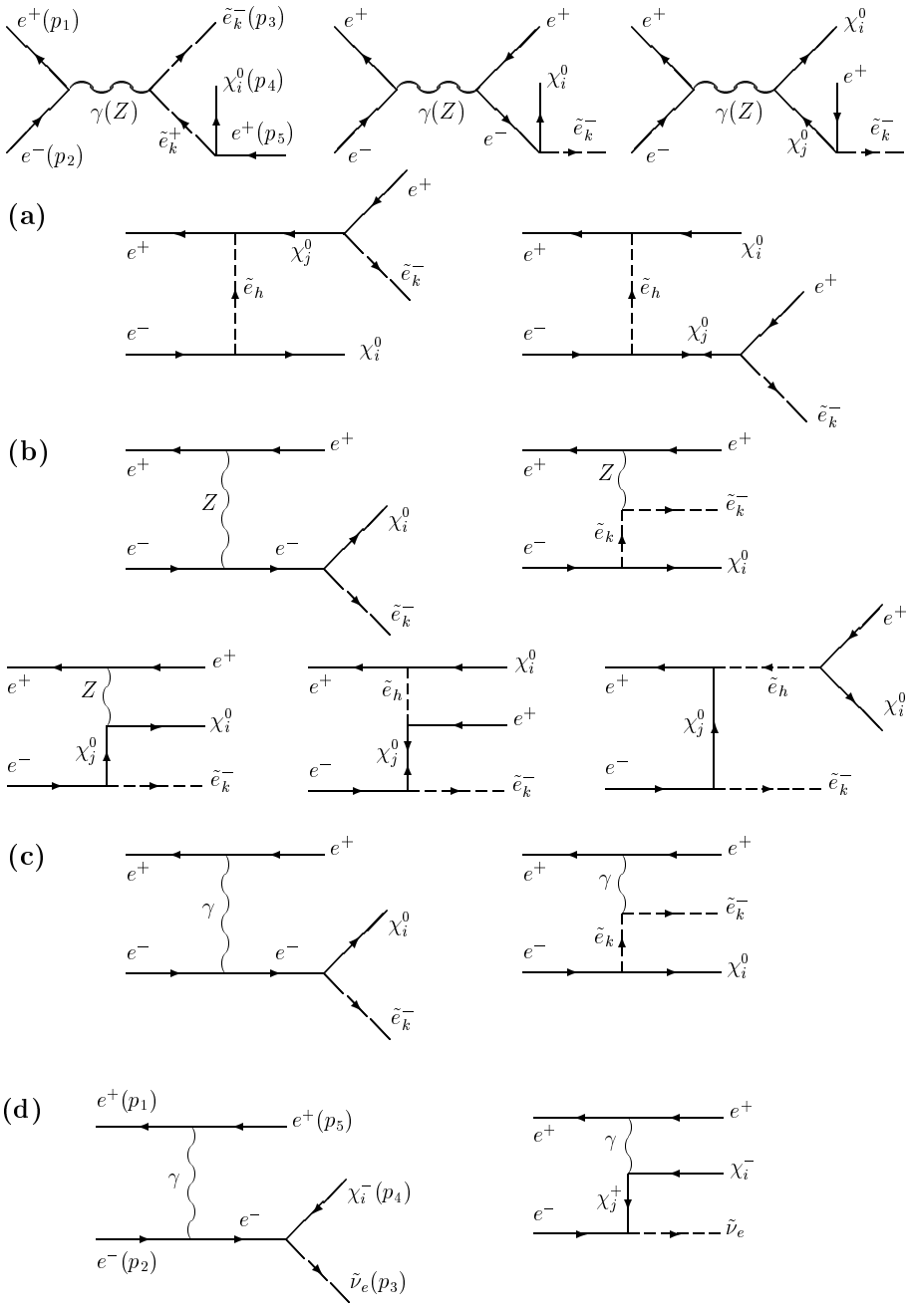

Fig. 3a-d. Feynman diagrams for the associated production of selectrons with neutralinos, $e^+e^- \to e^+\tilde{e}^-_{\rm L,R}\chi_i^0$: **a** universal diagrams, **b** non-universal t-channel diagrams without γ exchange and **c** diagrams with t-channel γ exchange; **d** is for diagrams with t-channel photon exchange for associated sneutrino–chargino production

tens of events per year in this case.] At $s^{1/2} = 1\,\text{TeV}$, the cross sections are in general smaller than that at a 500 GeV collider for a given ratio $m_{\tilde{\ell}}/s^{1/2}$ [with all the other parameters fixed] except in some cases where sleptons are produced in association with the heavier gaugino-like χ_2^0 and $\chi_1^\pm$ for which significantly larger regions of phase space are now available.

In Fig. 5, we display the cross sections at $s^{1/2} = 500\,\text{GeV}$ for a fixed value, $m_{\tilde{\ell}} \sim 275\,\text{GeV}$, as functions of the gaugino mass parameter M_2, i.e. for somewhat heavier $\chi_1^\pm$ and $\chi_{1,2}^0$ gaugino states. As expected, the cross sections decrease with larger M_2, in particular for associated slepton productions with heavier gauginos, χ_2^0 and $\chi_1^\pm$. In the case of $\tilde{e}_{\rm L,R}$ production with the LSP, where more phase space is available since $m_{\chi_1^0} \sim 0.5M_2$, the cross sections drop by less than a factor of 10 for a variation of M_2 from 100 to 250 GeV.

Finally, Fig. 6 shows the cross sections for the associated slepton production with the LSP at $s^{1/2} = 500\,\text{GeV}$ as functions of the slepton masses when the lighter neutralinos and chargino are almost higgsino-like (a) and mixtures of gauginos and higgsinos (b). For higgsino-like χ_1^0 particles the cross sections are much smaller than the previous case, a result of the smaller lepton–slepton–LSP coupling. In the case of mixed χ_1^0 states, the cross sections are slightly smaller than for a gaugino-like LSP. However, since all neutralinos and charginos will have comparable masses in this case, one has to consider the production

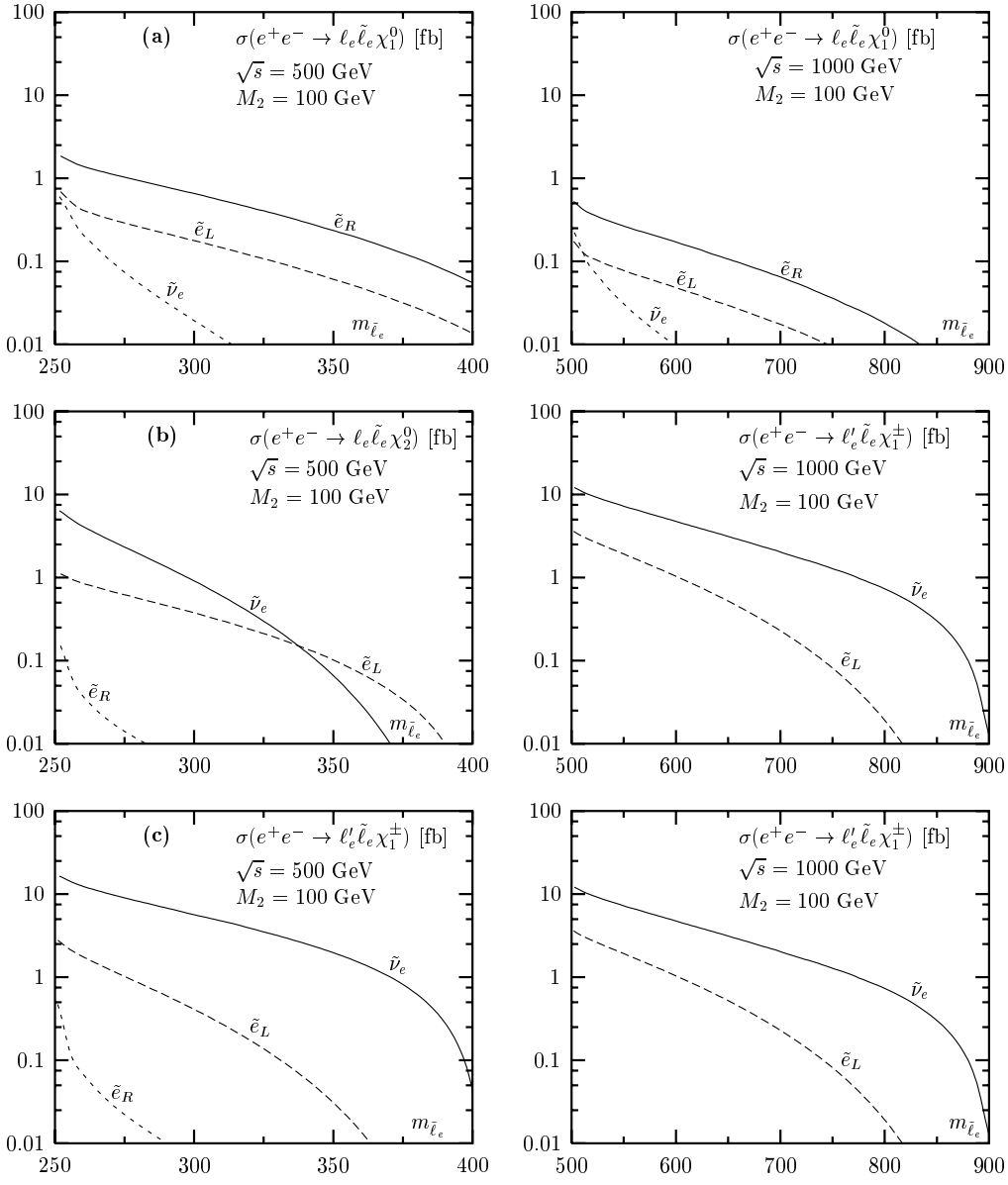

Fig. 4a–c. The total cross sections for the associated production processes of first generation sleptons and electroweak gauginos as functions of the slepton masses for center of mass energies of 500 GeV (left panels) and 1 TeV (right panels)

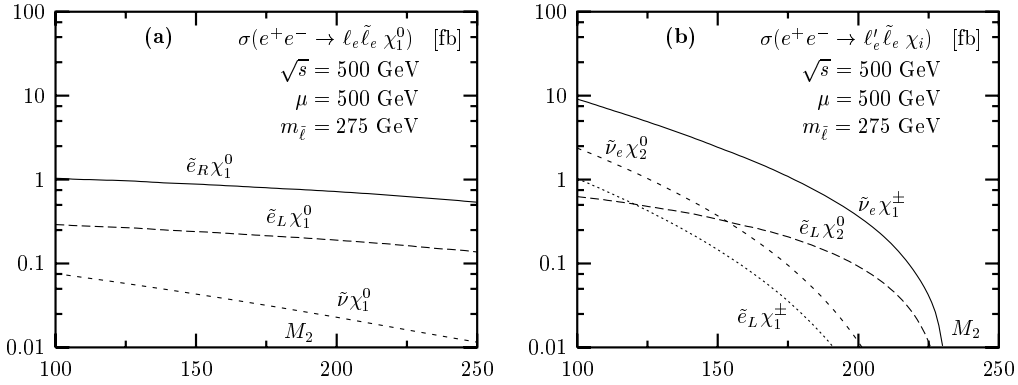

Fig. 5a,b. The total cross sections for the associated production of first generation sleptons with electroweak gauginos as functions of M_2 for $s^{1/2} = 500\,\text{GeV}$ and $m_{\tilde{\ell}} = 275\,\text{GeV}$

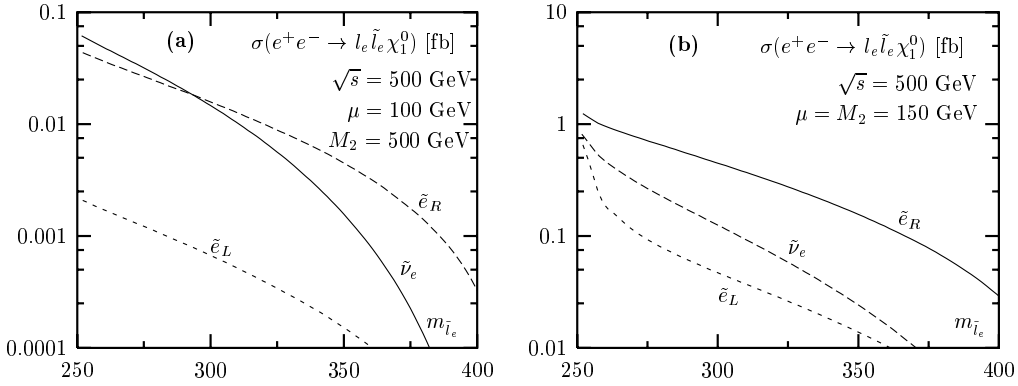

Fig. 6a,b. The total cross sections for the associated production of first generation sleptons with the lightest neutralino as a function of the slepton masses for $s^{1/2} = 500\,\text{GeV}$ for a higgsino-like χ_1^0 **a** and a mixed higgsino-gaugino χ_1^0 **b**

with the heavier χ particles. At the end of the day, once all processes have been included, the sum of the cross sections for the various processes will be similar in magnitude compared to the case of gaugino-like lightest neutralinos.

4 The total production cross sections

Let us now discuss the magnitude of the various contributions to the total associated cross section and the effects of the cut-off angle $\theta_{\min}$ which in the previous discussion was set to 1°. Taking as examples the associated production of the left- and right-handed selectrons with the LSP, $e^+e^- \to e^\pm\tilde{e}^\mp_{\text{L,R}}\chi_1^0$, we display in Table 1 the cross sections of the various contributions for a c.m. energy $s^{1/2} = 500\,\text{GeV}$ and the SUSY particle masses $m_{\tilde{e}_{\text{L,R}}} = 275\,\text{GeV}$ and $m_{\chi_1^0} \sim 75\,\text{GeV}$ [$M_2 = 150\,\text{GeV}$, $\mu = 500\,\text{GeV}$ and $\tan\beta = 30$], for several values of the cut-off angle $\theta_{\min}$. We will also compare these with the results obtained in the improved Weizsäcker–Williams approximation with a cut-off angle $\theta_c = \theta_{\min}$.

We define the "resonant" contribution to be the cross section from the two diagrams involving the t-channel exchange of the photon in Fig. 3c. As discussed previously, the sum of these two amplitudes is gauge invariant. These contributions strongly depend on the value of the cut-off angle $\theta_{\min}$ for the direction of the final electron (positron) with respect to the initial electron (positron) beams and which vetoes final leptons going in the very forward direction. The cross sections increase for decreasing cut-off angles. For instance, they are a factor of 2 to 3 larger for $\theta_{\min} \sim 0.5°$ than for $\theta_{\min} \sim 5°$, illustrating the fact that in most cases the final lepton goes down in the forward direction. However, for a small cut-off angle, we approach too closely the photon pole and the phase space integration becomes unstable numerically and when using a Monte Carlo method for such an integration, this actually calls for a very large number of integration points and commensurate number of iterations to achieve a stable result. An intermediate value, say $\theta_{\min} \sim 1°$ as used in the previous discussion, is more appropriate since the cross section is significant and at the same time its determination is more accurate.

Table 1. Variation of the contributions to the production cross section (in femtobarns) for the final states $e^\pm\tilde{e}^\mp_{\text{L}}\chi_1^0$ (upper table) and $e^\pm\tilde{e}^\mp_{\text{R}}\chi_1^0$ (lower table) with the cut-off angle $\theta_{\min}$ and comparison with the improved WW approximation with $\theta_c = \theta_{\min}$. The parameters are $s^{1/2} = 500\,\text{GeV}$, $m_{\tilde{e}_{\text{L,R}}} = 275\,\text{GeV}$, $M_2 = 150\,\text{GeV}$, $\mu = 500\,\text{GeV}$ and $\tan\beta = 30$

$\tilde{e}_{\text{L}}$

$\theta_c(\theta_{\min})$	IWW	Resonant	Non-resonant	Full	IWW+Full
5°	0.363	0.125	0.023	0.148	0.511
4°	0.355	0.135	0.023	0.158	0.513
3°	0.343	0.146	0.023	0.169	0.512
2°	0.327	0.164	0.023	0.187	0.514
1°	0.300	0.195	0.023	0.218	0.518
0.5°	0.272	0.220	0.023	0.243	0.515
0.2°	0.236	0.269	0.023	0.292	0.528
0.1°	0.209	0.294	0.023	0.317	0.526
0.05°	0.182	0.317	0.023	0.340	0.522

$\tilde{e}_{\text{R}}$

$\theta_c(\theta_{\min})$	IWW	Resonant	Non-resonant	Full	IWW+Full
5°	1.574	0.541	−0.062	0.479	2.053
4°	1.535	0.580	−0.062	0.518	2.053
3°	1.486	0.628	−0.062	0.566	2.052
2°	1.417	0.712	−0.062	0.650	2.067
1°	1.298	0.836	−0.063	0.773	2.071
0.5°	1.180	0.963	−0.063	0.900	2.080
0.2°	1.023	1.130	−0.063	1.067	2.090
0.1°	0.905	1.272	−0.063	1.209	2.114
0.05°	0.786	1.388	−0.063	1.325	2.111

The "non-resonant" contribution consists of the squared sum of the amplitudes of the diagrams which do not involve the t-channel photon, Fig. 3a,b [which forms also a gauge invariant set], and their interferences with the two diagrams in Fig. 3c. This interference does not involve any pole [since there are no $1/t^2$ terms] and is thus regular in the forward direction. As can be seen in Table 1, this contribution is rather small and does not depend strongly

on the cut-off angle $\theta_{\min}$ [provided that it is small enough]. The total cross section, i.e. the sum of the two contributions, is thus dominated by the resonant piece[2].

We have also displayed the $e^{\pm}\gamma \to \tilde{e}^{\pm}_{\rm L}\chi^0_1$ cross section in the improved Weizsäcker–Williams approximation [for unpolarized beams and including the two charge conjugate processes] with a cut-off angle $\theta_c = \theta_{\min}$. Here, the cross section decreases with decreasing angle since the probability of having the lepton emitted from the initial beam with a smaller angle is smaller, as is evident from (10).

In fact the "full" cross section and the cross section in the improved WW approximation are complementary, since they deal with complementary regions of the phase space for $\theta_c = \theta_{\min}$. The sum of the two gives the cross section for the associated production of sleptons and gauginos in the full angular range whether the final lepton is in the forward direction [i.e. experimentally undetected] or not. This sum, given in the last column of the table, is practically constant since it changes by less than $\sim 3\%$ between $\theta = 5^\circ$ and $\theta = 0.05^\circ$, while both of its components change by more than 100%. This modest shift is probably due to the fact that, at larger angles the improved WW approximation is rather poor, while at smaller angles, the three-body cross section is numerically unstable. A median value of $\theta \sim 1^\circ$, which has been adopted here, should therefore give an approximately good answer for the exclusive associated slepton+gaugino cross section[3].

5 Conclusions

In this paper, we have analyzed the associated production of first generation sleptons with neutralinos and charginos in the MSSM, at future high-energy e^+e^- colliders, extending the work done in [1]. We have discussed both the two-body particle production in the $e\gamma$ mode and the three-body particle production in the e^+e^- mode of the collider. In the latter case, we have shown that the production cross sections, thanks to a strong enhancement due to the presence of t-channel photon exchange contributions, can be rather large even for slepton masses significantly exceeding the kinematical two-body reach of the e^+e^- collider, i.e. $m_{\tilde{\ell}} > s^{1/2}/2$. This is particularly the case for the production of right-handed selectrons with the lightest neutralino and the production of sneutrinos with the lightest chargino, where slepton masses a few ten GeV beyond the beam energy can be probed if the electroweak gauginos are relatively light.

The final states discussed in this paper should be clear enough to be detected in the clean environment of e^+e^- colliders. However, to asses more firmly this possibility, a detailed study [15] of the signal and the various standard model backgrounds as well as the SUSY processes leading to the same final states [such as $\chi^+_1\chi^-_1$ and $\chi^0_1\chi^0_2$ pair production for which the cross sections can be large], has to be performed. In particular, since in the kinematical regions where the cross sections are large, a final state electron or positron goes in the direction of the beam pipe, large and dangerous backgrounds such as single W boson production or $\gamma\gamma$ collisions should be studied in detail. These studies are beyond the scope of this preliminary analysis and will be performed in the near future.

Acknowledgements. We thank Ayres Freitas and Peter Zerwas for clarifying discussions and E. Boos and A. Pukhov for their help in using CompHEP. AKD is supported by a MNERT fellowship while AD and MM are supported by the Eurogdr Supersymétrie and by the European Union under contract HPRN-CT-2000-00149.

Appendix

A The amplitudes of the various contributions

In this appendix, we present the amplitudes for the diagrams in Fig. 3b–d (the ones for the universal contributions, Fig. 3a, are given in [1]). The first two combined represent a generic set of extra Feynman diagrams for final states involving left- and right-handed selectron along with neutralinos (as compared to the set in Fig. 3a which is generic to all scalar final states), i.e. $e^+e^- \to \tilde{e}^-_{\rm L,R}e^+\chi^0_i$. The set of two diagrams in Fig. 3d are for the final state involving electronic sneutrino along with the chargino, i.e. $e^+e^- \to \tilde{\nu}_e e^+\chi^-_i$, and are the dominant ones containing photon poles when the outgoing positron is scattered in the very forward direction. In a covariant gauge, the amplitudes are given by

$$
\begin{aligned}
M_{b1} &= \frac{e^3/(s^3_{\rm W}c^2_{\rm W})}{\{(p_1-p_5)^2 - m^2_Z\}(p_1+p_2-p_5)^2} \\
&\times [\bar{v}_e(p_1)\gamma^\alpha(c^e_{\rm L}P_{\rm L} + c^e_{\rm R}P_{\rm R})v_e(p_5)] \\
&\times [\bar{u}_{\chi_i}(p_4)G^{Aik}_{b1}(\not{p}_1 + \not{p}_2 - \not{p}_5)\gamma_\alpha(c^e_{\rm L}P_{\rm L} + c^e_{\rm R}P_{\rm R})u_e(p_2)], \\
M_{b2} &= \frac{-e^3 a_{Z\tilde{e}_k\tilde{e}_k}/(s^3_{\rm W}c^2_{\rm W})}{\{(p_1-p_5)^2 - m^2_Z\}\{(p_1-p_3-p_5)^2 - m^2_{\tilde{e}_k}\}} \\
&\times [\bar{v}_e(p_1)(\not{p}_1 - \not{p}_5 - 2\not{p}_3)(c^e_{\rm L}P_{\rm L} + c^e_{\rm R}P_{\rm R})v_e(p_5)] \\
&\times [\bar{u}_{\chi_i}(p_4)G^{Aik}_{b2}u_e(p_2)], \\
M_{b3} &= \frac{-e^3/(s^3_{\rm W}c^2_{\rm W})}{\{(p_1-p_5)^2 - m^2_Z\}\{(p_2-p_3)^2 - m^2_{\chi_j}\}} \\
&\times [\bar{v}_e(p_1)\gamma^\alpha(c^e_{\rm L}P_{\rm L} + c^e_{\rm R}P_{\rm R})v_e(p_5)] \\
&\times \Big[\bar{u}_{\chi_i}(p_4)\gamma_\alpha(O^{ij}_{\rm L}P_{\rm L} + O^{ij}_{\rm R}P_{\rm R})
\end{aligned}
$$

[2] Note that the electron–photon vertex in the resonant contribution should be evaluated at $q^2 = 0$ and therefore $\alpha = 1/137$, while the other vertices should be evaluated at a scale close to $s^{1/2}$ and thus $\alpha \sim 1/128$ [13]. Also, in principle, one should use a running α; however, for our purpose, it is a good approximation to use the two values above. We thank E. Boos and T. Ohl for a discussion on this point

[3] This way of calculating the full cross section for multi-body final states involving photons in the t-channel, i.e. by calculating separately the cross section in the improved WW approximation in a narrow cone around the beam axis and the full multi-body process for the rest (which eliminates the numerical instabilities at small angles) and then performing the sum, has been discussed in the context of single W production at e^+e^- colliders [14]. This allows for fast Monte Carlo analyses

Table 2.

Diagrams	a_1	a_2	a_3	a_4	a_5	b_1	b_2	b_3	b_4	b_5	c_1	c_2
Relative signs	+	+	+	−	+	−	−	−	+	+	−	−

$$\times (\not{p}_2 - \not{p}_3 + m_{\chi_j}) G_{b3}^{Ajk} u_e(p_2)\Big],$$

$$M_{b4} = \left(\frac{e^3}{s_{\rm W}^3}\right) \sum_h \Big\{ \Big([\bar{v}_e(p_1) G_{b4}^{Bih} v_{\chi_i^0}(p_4)]$$
$$\times [\bar{v}_e(p_2) G_{b4}^{Ajk} (\not{p}_2 - \not{p}_3 - m_{\chi_j}) G_{b4}^{Ajh} v_e(p_5)] \Big)$$
$$\Big/ \Big(\{(p_1-p_4)^2 - m_{\tilde{e}_h}^2\} \{(p_2-p_3)^2 - m_{\chi_j}^2\} \Big) \Big\},$$

$$M_{b5} = -\left(\frac{e^3}{s_{\rm W}^3}\right) \sum_h \Big\{ \Big([\bar{v}_e(p_1) G_{b5}^{Bjh} (\not{p}_2 - \not{p}_3 + m_{\chi_j})$$
$$\times G_{b5}^{Ajk} u_e(p_2)] [\bar{u}_{\chi_i}(p_4) G_{b5}^{Aih} v_e(p_5)] \Big)$$
$$\Big/ \Big(\{(p_1+p_2-p_3)^2 - m_{\tilde{e}_h}^2\} \{(p_2-p_3)^2 - m_{\chi_j}^2\} \Big) \Big\}, \tag{A.1}$$

$$M_{c1(d1)} = \left(\frac{e^3}{s_{\rm W}}\right)$$
$$\frac{[\bar{v}_e(p_1)\gamma^\alpha v_e(p_5)][\bar{u}_{\chi_i}(p_4) G_{c1(d1)}^{Aik} (\not{p}_1 + \not{p}_2 - \not{p}_5)\gamma_\alpha u_e(p_2)]}{(p_1-p_5)^2 (p_1+p_2-p_5)^2},$$

$$M_{c2} = -\left(\frac{e^3}{s_{\rm W}}\right)$$
$$\frac{[\bar{v}_e(p_1)(\not{p}_1 - \not{p}_5 - 2\not{p}_3)\, v_e(p_5)][\bar{u}_{\chi_i}(p_4) G_{c2}^{Aik} u_e(p_2)]}{(p_1-p_5)^2 \{(p_1-p_3-p_5)^2 - m_{\tilde{e}_k}^2\}},$$

$$M_{d2} = \left(\frac{e^3}{s_{\rm W}}\right)$$
$$\frac{[\bar{v}_e(p_1)\gamma^\alpha v_e(p_5)][\bar{u}_{\chi_i}(p_4)\gamma_\alpha (\not{p}_1 - \not{p}_4 - \not{p}_5 - m_{\chi_j}) G_{d2}^{Ajk} u_e(p_2)]}{(p_1-p_5)^2 \{(p_1-p_4-p_5)^2 - m_{\chi_j}^2\}}. \tag{A.2}$$

The relative signs among different diagrams contributing to the same final state arising out of the anticommuting nature of the fermionic fields (Wick's theorem) are summarized in Table 2.

We try to keep the conventions of our previous paper [1] in defining the variables and constants more or less intact. $P_{\rm L,R} = (1/2)(1 \mp \gamma_5)$ are the left- and right-handed chirality projectors, $e^2 = 4\pi\alpha$ with α being the fine structure constant, $s_{\rm W} = \sin\theta_{\rm W}$ and $c_{\rm W} = \cos\theta_{\rm W}$ are the sine and the cosine of the Weinberg angle, while $T_{3,\tilde{e}_k(e)}$ and $Q_{\tilde{e}_k(e)}$ are the third component of the weak isospin and the charge of the kth chiral selectron (electron). The couplings of electron and selectrons with gauge bosons are parametrized by

$$c_{\rm L}^e = T_{3,e} - Q_e s_{\rm W}^2, \quad c_{\rm R}^e = -Q_e s_{\rm W}^2,$$
$$a_{Z\tilde{e}_k\tilde{e}_k} = T_{3,\tilde{e}_k} - Q_{\tilde{e}_k} s_{\rm W}^2, \tag{A.3}$$

where $k = {\rm L}, {\rm R}$ is the chirality of the selectron, while the neutralino-neutralino–Z boson couplings are parametrized by

$$O_{ij}^{\rm L} = -O_{ij}^{\rm R} = -\frac{1}{2} N_{i3} N_{j3} + \frac{1}{2} N_{i4} N_{j4} \tag{A.4}$$

following the notations of Gunion and Haber [7]. As in [1], for the fermion–sfermion–gaugino couplings we follow Figs. 22, 23 and 24 of [7]. In the amplitudes presented in (A.1) and (A.2), the couplings G absorb the sign on the imaginary i's as shown against the vertices in the figures mentioned above. The subscripts of G indicate the diagram while superscripts (i or j) indicate whether the coupling is arising at a vertex with an outgoing (i) or a propagator (j) gaugino. A superscript $k(h) = {\rm L}, {\rm R}$ indicates the chirality of the sfermion in the final state (or in the scalar propagator) as appropriate for the vertex in context. G couplings with superscripts A and B are related by hermitian conjugation at the Lagrangian level, while involving the same set of fields in respective cases. In all the couplings defined above we have taken the neutralino-mixing matrix N in the B–W^3 basis, the neutralino-mixing matrix N' in the $\tilde{\gamma}$–$\tilde{Z}$ basis, the two chargino-mixing matrices U and V, to be real as is appropriate in an analysis that conserves CP.

The following are the couplings in detail:

$$G_{\rm (Diag.)}^{Ai(j)({\rm L,R},\tilde{\nu})} = C_{\rm L(R)}^A (A_{1({\rm L,R},\tilde{\nu})}^{i(j)} P_{\rm L} + A_{2({\rm L,R},\tilde{\nu})}^{i(j)} P_{\rm R}),$$
$$G_{\rm (Diag.)}^{Bi(j){\rm L(R)}} = C_{\rm L(R)}^B (B_{1{\rm L(R)}}^{i(j)} P_{\rm R} + B_{2{\rm L(R)}}^{i(j)} P_{\rm L}), \tag{A.5}$$

The generic values and structures of the terms on the right hand side of the above equations are defined below in reference to final states with neutralino and with chargino. For final states with neutralinos, one has

$$C_{\rm L(R)}^A = C_{\rm L(R)}^B = -1,$$
$$A_{i(j)1{\rm L}} = B_{i(j)1{\rm L}}$$
$$= -\sqrt{2}\left[s_{\rm W} N'_{i(j)1} + \left(\frac{1}{2} - s_{\rm W}^2\right) N'_{i(j)2} \right],$$
$$A_{i(j)2R} = B_{i(j)2R} = \sqrt{2}(s_{\rm W} N'_{i(j)1} - s_{\rm W}^2 N'_{i(j)2}),$$
$$A_{i(j)2L} = A_{i(j)1{\rm R}} = B_{i(j)2L} = B_{i(j)1{\rm R}}$$
$$= \frac{m_e}{\sqrt{2} m_W} \left(\frac{N_{i(j)3}}{\cos\beta} \right). \tag{A.6}$$

[Note that we have neglected the very small mixing in the selectron sector although retained the small electron mass (m_e) in the above couplings; the reason behind this is discussed in Appendix B.] For final states with charginos, as in case for the Feynman diagrams in Fig. 3d, one has

$$C_{\rm L}^A = -C_{\rm L}^B = +1, \quad C_{\rm R}^A = C_{\rm R}^B = 0,$$
$$A_{i(j)1} = V_{i(j)1}, \quad A_{i(j)2} = -\frac{m_e}{\sqrt{2} m_W} \left(\frac{U_{i(j)2}}{\cos\beta} \right),$$
$$B_{jl} = A_{jl}, \quad \text{with} \quad l = 1, 2. \tag{A.7}$$

In the present analysis we do not use the sparticle widths, and hence, have to impose kinematic constraints to avoid situations closely approaching the on-shell limits for the (sfermion and/or gaugino) propagators that would have led to resonances. In [1] we have justified this consideration and illustrated with concrete examples the importance of including sparticle widths when approaching such thresholds.

B The differential cross section

In this appendix, we present the analytical expressions of the differential cross section for the following two associated production processes:

$$e^+(p_1)e^-(p_2) \to \tilde{e}_k^-(p_3)\chi_i^0(p_4)e^+(p_5), \qquad \text{(B.1)}$$
$$e^+(p_1)e^-(p_2) \to \tilde{\nu}(p_3)\chi_i^-(p_4)e^+(p_5), \qquad \text{(B.2)}$$

where $k = \mathrm{L}, \mathrm{R}$ is the handedness of the produced selectron. We have considered the (gauge invariant) sets of only two Feynman diagrams, Fig. 3c,d, i.e. for the processes which contain the photon pole in the t-channel. This is a reasonably good approximation, as demonstrated in Table 1, for the "full" cross section.

Due to the presence of forward poles in these diagrams, we have to keep the electron mass in our analysis which ultimately regulates this singular behavior of the scattering matrix element over the appropriate phase space. However, it is sufficient to retain the terms proportional to m_e^2/t_1^2, where m_e is the mass of the electron and t_1 is the square of the 4-momentum transfer between the incoming and outgoing positron. Elsewhere it is safe to take $m_e \to 0$. Hence, in the following expressions for the diagonal and interference terms we have made two parts explicit; one proportional to m_e^2/t_1^2 and the other not. We ignored, however, the negligible mixing in the selectron sector.

The complete spin-averaged matrix element squared is given by

$$|\mathcal{M}|^2 = 4\frac{(4\pi\alpha)^3}{s_{\mathrm{W}}^2}\sum_{i,j=1,2} T_{ij}, \qquad \text{(B.3)}$$

where α is the fine structure constant [to be evaluated at the scale of the momentum transfer at the vertex]. The T_{ij}'s are the squared amplitudes and the interferences for the two diagrams in Fig. 3c (and 3d). The effects of permutations of suffixes for the interferences are already included in the original terms and hence such permutations are to be left out.

The diagonal terms are given by

$$T_{c_1(d_1)} = \frac{1}{s_2^2}\left[\frac{A_{i1k}^2}{t_1^2}(\mathcal{A}_1+\mathcal{A}_2+\mathcal{A}_3) - \frac{m_e^2}{t_1^2}\left\{A_{i1k}^2\mathcal{A}_4 - \frac{A_{i2k}^2}{m_W^2}(\mathcal{A}_1+\mathcal{A}_2)\right\}\right],$$

$$T_{c_2} = \frac{-2}{(m_{\chi_i}^2 - s_2 + t_1 - t_2)^2} \times \left[\frac{A_{i1k}^2}{t_1^2}\mathcal{B}_1\left(\mathcal{B}_2\mathcal{B}_3 + m_{\tilde{f}}^2 t_1\right) - \frac{m_e^2}{t_1^2}\left\{4A_{i1k}\left(\frac{A_{i2k}}{m_W}\right)\mathcal{B}_3 + \left\{\left(\frac{A_{i2k}}{m_W}\right)^2\mathcal{B}_3 - A_{i1k}^2\right\}\mathcal{B}_4\right\}\right],$$

$$T_{d_2} = \frac{1}{(t_2 - m_{\chi_j}^2)^2} \times \left[\frac{A_{j1k}^2}{t_1^2}\{\mathcal{C}_1 + (\mathcal{C}_2+\mathcal{C}_3+\mathcal{C}_4+\mathcal{C}_5+\mathcal{C}_6)t_1\} - \frac{m_e^2}{t_1^2}\left\{8A_{j1k}\left(\frac{A_{j2k}}{m_W}\right)\mathcal{C}_7 - \left(\frac{A_{j2k}}{m_W}\right)^2\mathcal{C}_5 - A_{j1k}^2(\mathcal{C}_2 + 2\mathcal{C}_3 - 2\mathcal{C}_4 - 3\mathcal{C}_5 + \mathcal{C}_8)\right\}\right], \qquad \text{(B.4)}$$

while the interference terms are given by

$$T_{c_1c_2} = \frac{1}{s_2(m_{\chi_i}^2 - s_2 + t_1 - t_2)} \times \left[\frac{A_{i1k}^2}{t_1^2}\{\mathcal{D}_1 + \mathcal{D}_2 + m_{\chi_i}^2(\mathcal{D}_3+\mathcal{D}_4) + m_{\tilde{f}}^2(\mathcal{D}_5+\mathcal{D}_6)\} - \frac{m_e^2}{t_1^2}\left\{A_{i1k}\left(2\frac{A_{i2k}}{m_W}m_{\chi_i}\mathcal{D}_7 - A_{i1k}\mathcal{D}_8\right) + \frac{A_{i2k}}{m_W}\left(2m_{\chi_i}A_{i1k}\mathcal{D}_7 + \frac{A_{i2k}}{m_W}(\mathcal{D}_1+\mathcal{D}_3+\mathcal{D}_5)\right)\right\}\right],$$

$$T_{d_1d_2} = \frac{-1}{s_2(m_{\chi_j}^2 - t_2)} \times \left[\frac{A_{i1k}A_{j1k}}{t_1^2}\{\mathcal{F}_1 + \mathcal{F}_2 + m_{\chi_i}^2(\mathcal{F}_3+\mathcal{F}_4) + m_{\tilde{f}}^2(\mathcal{F}_5+\mathcal{F}_6)\} - \frac{m_e^2}{t_1^2}\left\{A_{i1k}\left(2\frac{A_{j2k}}{m_W}m_{\chi_i}\mathcal{F}_7 - A_{j1k}\mathcal{F}_8\right) + \frac{A_{i2k}}{m_W}\left(2m_{\chi_i}A_{j1k}\mathcal{F}_7 + \frac{A_{j2k}}{m_W}(\mathcal{F}_1+\mathcal{F}_3+\mathcal{F}_5)\right)\right\}\right]. \qquad \text{(B.5)}$$

The factors $\mathcal{A}_i$, $\mathcal{B}_i$, $\mathcal{C}_i$, $\mathcal{D}_i$, are given below:

$$\mathcal{A}_1 = s\left\{(m_{\chi_i}^2 - m_{\tilde{f}}^2)(2s - s_2) + m_{\tilde{f}}^2 s_2\right\},$$
$$\mathcal{A}_2 = s_2\left[s\{2(s - s_1 - s_2) + t_2\} + s_2(s_1 - t_2)\right],$$
$$\mathcal{A}_3 = t_1\left\{(m_{\chi_i}^2 - m_{\tilde{f}}^2)(2s - s_2 + t_1) + s_2(s - s_1 + t_2)\right\},$$
$$\mathcal{A}_4 = 6s(m_{\chi_i}^2 - m_{\tilde{f}}^2) + s_2\left\{4(m_{\tilde{f}}^2 + s) - 3(s_1 + s_2) - t_2\right\},$$
$$\mathcal{B}_1 = m_{\tilde{f}}^2 - s_2 + t_1 - t_2,$$
$$\mathcal{B}_2 = m_{\chi_i}^2 + s - s_1 - s_2,$$
$$\mathcal{B}_3 = s - s_1 + t_2,$$
$$\mathcal{B}_4 = -m_{\tilde{f}}^2 + s_2 + t_2,$$
$$\mathcal{C}_1 = -2m_{\tilde{f}}^2 s_1^2 + s_1\{2(m_{\tilde{f}}^2 - s + s_1) + s_2\}t_2$$

$$
\begin{aligned}
&+ (s - 2s_1 - s_2)t_2^2 \\
&+ m_{\chi_j}^2(2ss_1 - s_1s_2 - st_2 + s_2t_2) \\
&+ m_{\chi_i}^2\{-m_{\chi_j}^2 s + 2m_{\tilde{f}}^2(s_1 - t_2) + t_2(s - 2s_1 + 2t_2)\}, \\
\mathcal{C}_2 &= -m_{\chi_j}^2(s_2 + t_2) + s_2t_2, \\
\mathcal{C}_3 &= -2m_{\chi_i}m_{\chi_j}(m_{\tilde{f}}^2 - t_2), \\
\mathcal{C}_4 &= m_{\chi_j}^2 s - m_{\tilde{f}}^2(2s_1 - t_2) - st_2, \\
\mathcal{C}_5 &= s_1(m_{\chi_j}^2 + t_2), \\
\mathcal{C}_6 &= m_{\chi_i}^2 m_{\tilde{f}}^2 - (m_{\chi_i}^2 - m_{\chi_j}^2 + m_{\tilde{f}}^2)t_1, \\
\mathcal{C}_7 &= m_{\chi_j}(m_{\chi_i}^2 - s_1)(s_1 - t_2), \\
\mathcal{C}_8 &= 2\{m_{\chi_j}^2(m_{\chi_i}^2 + m_{\tilde{f}}^2) - m_{\chi_i}^2 s_1 + s_1^2\} + t_2^2, \\
\mathcal{D}_1 &= m_{\chi_i}^4 s + 2s^2(2s_2 + t_2) + s_2(s_1 - t_2)(2s_1 + 3s_2 + t_2) \\
&+ s\left\{-4s_2^2 + s_2t_2 + t_2^2 - 2s_1(3s_2 + t_2)\right\}, \\
\mathcal{D}_2 &= -t_1\left\{2m_{\tilde{f}}^4 + (s - s_1)(2s - 2s_1 - 3s_2)\right. \\
&+ \left.(s - s_1 - 2s_2)t_2\right\}, \\
\mathcal{D}_3 &= -2m_{\tilde{f}}^2 s + (2s + s_2)\,(s - s_1 + t_2), \\
\mathcal{D}_4 &= t_1\,(m_{\tilde{f}}^2 - s + s_1 - 2t_2), \\
\mathcal{D}_5 &= -4s^2 + 4s(s_1 + s_2) - 2st_2 - 2s_2(s_1 - t_2), \\
\mathcal{D}_6 &= t_1(-2s + 2s_1 + 3s_2 - 2t_1 + t_2), \\
\mathcal{D}_7 &= m_{\chi_i}^2 s + 2s^2 + s_2(s_1 - t_2) - s\left\{2(s_1 + s_2) - t_2\right\}, \\
\mathcal{D}_8 &= 2m_{\chi_i}^4 + 2ss_1 - 2s_1^2 + 6ss_2 - 6s_1s_2 - 5s_2^2 + 3st_2 \\
&- s_1t_2 - s_2t_2 + t_2^2 + m_{\chi_i}^2(-4m_{\tilde{f}}^2 + 3s - s_1 + s_2 + t_2) \\
&- 2m_{\tilde{f}}^2\left\{4s - 3(s_1 + s_2) + t_2\right\}, \\
\mathcal{F}_1 &= -m_{\chi_i}^4 s + 4m_{\chi_i}m_{\chi_j}s(s + s_2) - s_1s_2(-2s + 2s_1 + s_2) \\
&+ (2s + s_2)(-s + s_1 + s_2)t_2 + (-s + s_2)t_2^2, \\
\mathcal{F}_2 &= t_1\{2m_{\tilde{f}}^4 + 2m_{\chi_i}m_{\chi_j}(2s - s_2 + t_1) \\
&+ (s - s_1)(2s - 2s_1 - s_2 + t_2)\}, \\
\mathcal{F}_3 &= 2m_{\tilde{f}}^2 s - 2s^2 + s_2(s_1 - t_2) + 2s(s_1 + s_2 - t_2), \\
\mathcal{F}_4 &= t_1(-m_{\tilde{f}}^2 - s_1 + s + 2t_2), \\
\mathcal{F}_5 &= -2\{(s_1 - t_2)(s - s_2) + ss_1\}, \\
\mathcal{F}_6 &= -t_1\{2(s + s_1) + (s_2 + t_2)\}, \\
\mathcal{F}_7 &= -\{s(m_{\chi_i}^2 - s_1) - (s - s_2)(s_1 - t_2)\}, \\
\mathcal{F}_8 &= -2m_{\chi_i}^4 - 2ss_1 + 2s_1^2 + 4m_{\chi_i}m_{\chi_j}(3s - s_2) \\
&+ 2ss_2 - s_2^2 \\
&+ m_{\chi_i}^2(4m_{\tilde{f}}^2 - 3s + s_1 + 3s_2 - t_2) \\
&- 3st_2 + s_1t_2 - s_2t_2 - t_2^2 \\
&+ 2m_{\tilde{f}}^2(-2s - 3s_1 + s_2 + t_2),
\end{aligned}
\tag{B.6}
$$

where the 5 Lorentz invariant Byckling–Kajantie (Mandelstam-analogue) [16] variables for a $(2 \to 3)$ process are given (in terms of 4-momenta) by

$$
\begin{aligned}
s &= (p_1 + p_2)^2, \quad s_1 = (p_4 + p_5)^2, \\
s_2 &= (p_3 + p_4)^2, \quad t_1 = (p_1 - p_5)^2,
\end{aligned}
$$

$$
t_2 = (p_2 - p_3)^2, \tag{B.7}
$$

A_{ink} are the couplings of the ith gaugino with a sfermion of chirality k and a fermion. $n = 1, 2$, where 1 gives the coupling with SU(2) and U(1) gaugino content of the eigenstate and 2 gives the one with the higgsino part and proportional to the electron mass. $A_{i(j)nk} = A_{i(j)n}$ for $\tilde{\nu}$ final states as in Fig. 3d. Also we have used the scaled $A_{i(j)2k}$ and $A_{i(j)2}$ in Appendix B which are equal to $A_{i(j)2k}$ in (A.6) and $A_{i(j)2}$ in (A.7), respectively, but divided by m_e. This is done to make the m_e dependences of the squared amplitudes explicit which is important for our purpose (as discussed in the beginning of this appendix), rather than keeping it concealed under the definitions of the couplings. Note that the mass dimensions of the variables $\mathcal{A}_i$, $\mathcal{B}_i$, $\mathcal{C}_i$, $\mathcal{D}_i$ and $\mathcal{F}_i$ are left arbitrary to render the expressions for the squared terms T_{ij} into a somewhat systematic look.

The differential cross section is obtained by dividing by the flux and multiplying by the phase space,

$$
\begin{aligned}
\mathrm{d}\sigma = &\frac{1}{2s}\frac{1}{(2\pi)^5}\frac{\mathrm{d}^3p_3}{2E_3}\frac{\mathrm{d}^3p_4}{2E_4}\frac{\mathrm{d}^3p_5}{2E_5} \\
&\times \delta^4(p_1 + p_2 - p_3 - p_4 - p_5)|M|^2.
\end{aligned}
\tag{B.8}
$$

The integral over the phase space is then performed numerically in order to obtain the total production cross section.

Finally, we note that the production of the charged conjugate states has also to be taken into account. Due to CP-invariance, these cross sections are the same as for the corresponding previous ones, which have thus to be multiplied just by a factor of 2.

References

1. A. Datta, A. Djouadi, Eur. Phys. J. C **25**, 523 (2002)
2. F.M. Renard, Z. Phys. C **14**, 209 (1982); J.A. Grifols, R. Pascual, Phys. Lett. B **142**, 455 (1984); B **135**, 319 (1984); M. Drees, K. Grassie, Z. Phys. C **28**, 451 (1985)
3. F. Cuypers, G. van Oldenborgh, R. Ruckl, Nucl. Phys. B **409**, 144 (1993); D. Choudhury, F. Cuypers, Nucl. Phys. B **451**, 16 (1995); S. Hesselbach, H. Fraas, Phys. Rev. D **55**, 1343 (1997); V. Barger, T. Han, J. Kelly, Phys. Lett. B **419**, 233 (1998); C. Blochinger, H. Fraas, Acta Phys. Polon. B **30**, 3417 (1999)
4. C.F. Weizsäcker, Z. Phys. C **88**, 612 (1934); E.J. Williams, Phys. Rev. D **45**, 729 (1934)
5. S. Frixione, M.L. Mangano, P. Nason, G. Ridolfi, Phys. Lett. B **319**, 339 (1993)
6. I. Ginzburg, G. Kotkin, V. Serbo, V. Telnov, Nucl. Instrum. Meth. **205**, 47 (1983); **219**, 5 (1984); V. Telnov, Nucl. Instrum. Meth. A **294**, 72 (1990); A **335**, 3 (1995); J. Kühn, E. Mirkes, J. Steegborn, Z. Phys. C **57**, 615 (1993)
7. J. Gunion, H. Haber, Nucl. Phys. B **272**, 1 (1986), (E) hep-ph/9301205
8. For the couplings see also A. Djouadi, J. Kalinowski, P. Ohmann, P.M. Zerwas, Z. Phys. C **74**, 93 (1997); P.M. Zerwas (editor) et al., hep-ph/9605437

9. ECFA/DESY Photon Collider Working Group, DESY-2001-011, hep-ex/0108012
10. E. Accomando, Phys. Rept. **299**, 1 (1998); American Linear Collider Working Group (T. Abe et al.), Report SLAC-R-570 and hep-ex/0106057; J. Bagger et al., hep-ex/0007022; H. Murayama, M. Peskin, Ann. Rev. Nucl. Part. Sci. **46**, 533 (1996); TESLA TDR, Part III: Physics at e^+e^- Linear Collider, D. Heuer, D. Miller, F. Richard, edited by P.M. Zerwas et al., Report DESY-01-011C, hep-ph/0106315
11. For a summary on the experimental limits of the masses of the Higgs and SUSY particles, see F. Gianotti, talk given at the EPS-HEP-2001, 12–18 July, Budapest
12. A. Pukhov, E. Boos, M. Dubinin, V. Edneral, V. Ilyin, D. Kovalenko, A. Kryukov, V. Savrin, S. Shichanin, A. Semenov, CompHEP – a package for evaluation of Feynman diagrams and integration over multi-particle phase space. User's manual for version 33, Preprint INP MSU 98-41/542, hep-ph/9908288
13. E. Boos, T. Ohl, Phys. Rev. Lett. **83**, 480 (1999)
14. See for instance: G. Passarino, hep-ph/9810416; E.E. Boos, M.N. Dubinin, hep-ph/9909214
15. For some examples of such studies, see A. Freitas, D.J. Miller, P.M. Zerwas, Eur. Phys. J. C **21**, 361 (2001); J.L. Feng, M.E. Peskin, Phys. Rev. D **64**, 115002 (2001)
16. E. Byckling, K. Kajantie, Phys. Rev. D **187**, 2008 (1969); F.M. Renard, in Electron Positron Collisions (Editions Frontièrs, Gif-sur-Yvette 1981)